

## Supporting Information

# Facet-dependent Carrier Dynamics of Cuprous Oxide Regulating the Photocatalytic Hydrogen Generation

*Cui Ying Toe, Marlene Lamers, Thomas Dittrich, Hassan A. Tahini, Sean C. Smith, Jason Scott, Rose Amal, Roel van de Krol, Fatwa F. Abdi\*, Yun Hau Ng\**

Dr. C. Y. Toe, Assoc. Prof. J. Scott, Prof. R. Amal, Assoc. Prof. Y. H. Ng  
Particles and Catalysis Research Group, School of Chemical Engineering, The University of  
New South Wales, NSW 2052, Australia.

Dr. M. Lamers, Prof. R. van de Krol, Dr. F. F. Abdi  
Institute for Solar Fuels, Helmholtz-Zentrum Berlin für Materialien und Energie GmbH,  
Hahn-Meitner-Platz 1, Berlin 14109, Germany.

Dr. T. Dittrich  
Institute for Silicon Photovoltaics, Helmholtz-Zentrum Berlin für Materialien und Energie  
GmbH, Kekuléstrasse 5, Berlin 12489, Germany.

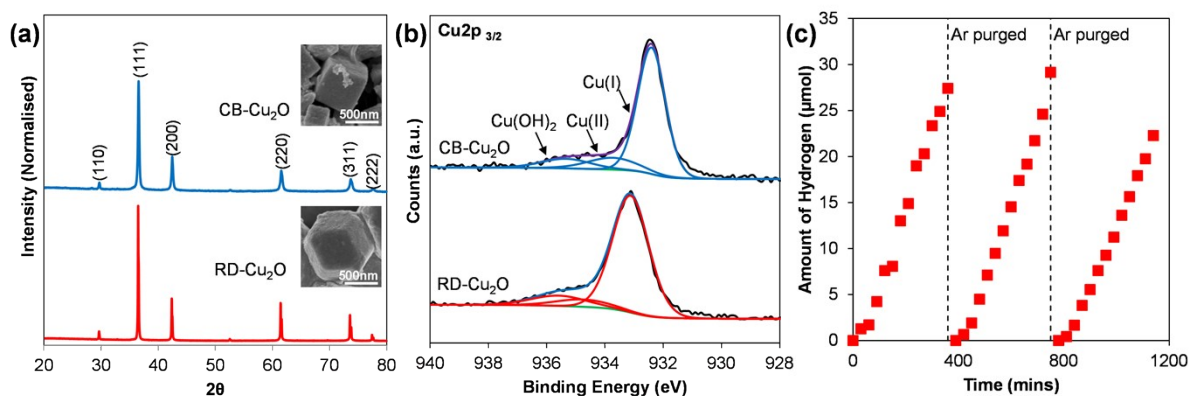
Dr. H. Tahini, Prof. S. C. Smith  
Research School of Physics and Engineering, The Australian National University, Canberra,  
ACT 2601, Australia.

Assoc. Prof. Y. H. Ng  
School of Energy and Environment, City University of Hong Kong, Kowloon, Hong Kong  
SAR, P. R. China.

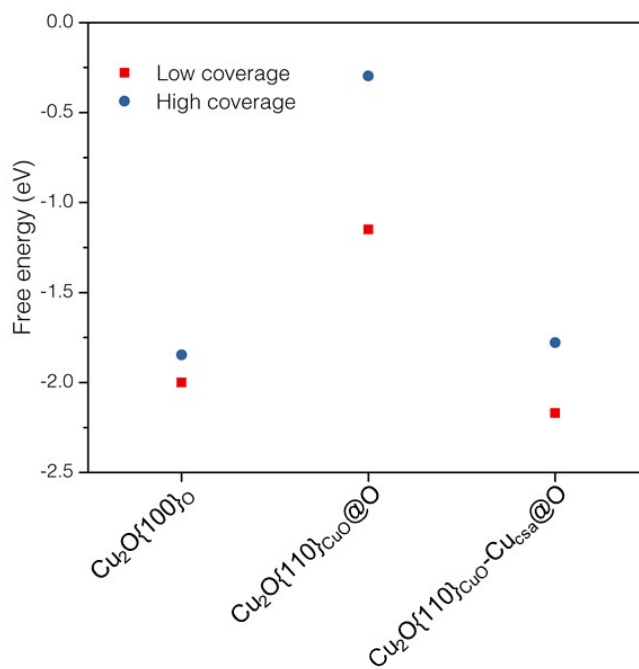
Email: [yunhau.ng@cityu.edu.hk](mailto:yunhau.ng@cityu.edu.hk)

**Table S1:** Comparison table of photocatalytic H<sub>2</sub> evolution rate of pristine Cu<sub>2</sub>O photocatalysts with cubic and polyhedral morphologies.

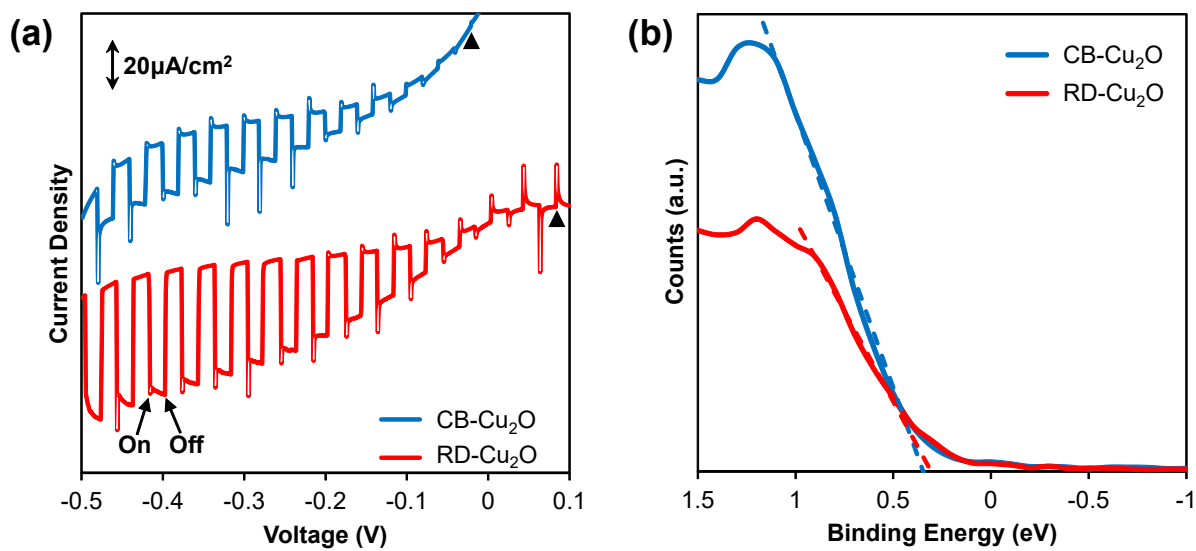
Photocatalyst	Morphology	Hole scavenger	Lamp	H <sub>2</sub> evolution rate (μmol g <sup>-1</sup> h <sup>-1</sup> )	Ref.
Cu <sub>2</sub> O	Cubic	Glucose solution	300 W Xe lamp with 420 nm cut-off filter	8.8	S1
Cu <sub>2</sub> O	Cubic	20 v/v% Methanol	300 W Xe lamp	4.9	S2
Cu <sub>2</sub> O	Cubic	17 v/v% Triethanola mine	300 W Xe lamp	87.5	S3
Cu <sub>2</sub> O	Cubic	25 v/v% Methanol	300 W Xe lamp with 550 nm cut-off filter, 100 mW cm <sup>-2</sup>	16.8	S4
Cu <sub>2</sub> O	Cubic	0.5 M Na <sub>2</sub> SO <sub>3</sub>	300 W Xe lamp, 385 mW cm <sup>-2</sup>	65	This work
Cu <sub>2</sub> O	Polyhedron	Glucose solution	300 W Xe lamp with 420 nm cut-off filter	12.3	S1
Cu <sub>2</sub> O	Rhombic Dodecahedral	-	300 W Xe lamp	1.6	S5
Cu <sub>2</sub> O	Rhombic Dodecahedral	0.5 M Na <sub>2</sub> SO <sub>3</sub>	300 W Xe lamp, 385 mW cm <sup>-2</sup>	99	This work



**Figure S1.** (a) XRD patterns with insets SEM images and (b) XPS spectra after 6 h of illumination of CB-Cu<sub>2</sub>O and RD-Cu<sub>2</sub>O. The difference in corrosion tendencies between the two Cu<sub>2</sub>O samples with distinct exposed facets was assumed to be minimal. Although the crystallite size of CB-Cu<sub>2</sub>O after reaction was slightly decreased from 59 nm to 41 nm (this also leads to the negative shift of Cu<sub>2</sub>p<sub>3/2</sub> peaks to lower binding energy),<sup>S6</sup> morphological properties, crystal structures and surface Cu chemical compositions of the post-reaction samples were retained, as observed in the above XRD, SEM and X-ray photoelectron spectroscopy (XPS) spectra. (c) Long-term photocatalytic H<sub>2</sub> evolution reaction of RD-Cu<sub>2</sub>O. The reactor system was re-purged with Argon gas every 6 hours of illumination. The performance of RD-Cu<sub>2</sub>O was retained at more than 80 % after the third cycle of reaction. Although the performance during the third cycle is marginally reduced, utilization of Na<sub>2</sub>SO<sub>3</sub> hole scavenger has shown to improve the photostability.<sup>S7</sup> Therefore, this improvement (though not extensive) is enough to allow for characterization and comparison of the intrinsic charge properties of CB- Cu<sub>2</sub>O and RD- Cu<sub>2</sub>O.



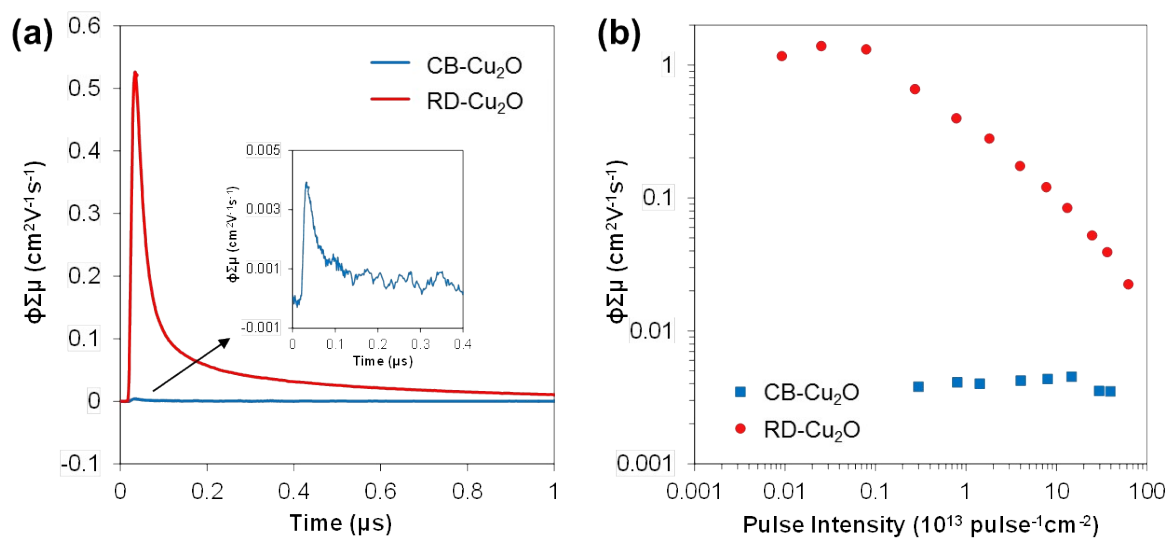
**Figure S2:** The low and high coverage free energies of H\* on Cu<sub>2</sub>O{100} and Cu<sub>2</sub>O{110} surfaces.



**Figure S3:** (a) Linear sweep voltammetry measured from 0.1 to -0.5 V vs. Ag/AgCl and (b) valence band XPS measurement of CB-Cu<sub>2</sub>O and RD-Cu<sub>2</sub>O.

**Table S2:** Electronic properties of CB-Cu<sub>2</sub>O and RD-Cu<sub>2</sub>O.

Samples	Bandgap (eV)	On-set potential/ Fermi Level (V)		Potential difference from XPS	Valence	Conduction
		vs.			Band	Band
		Ag/AgCl pH $\sim$ 7	vs. NHE pH=0		Maximum (eV)	Minimum (eV)
CB-Cu <sub>2</sub> O	2.02	-0.02	0.59	0.35	+0.94	-1.08
RD-Cu <sub>2</sub> O	2.00	0.08	0.69	0.31	+1.00	-1.00

**Figure S4:** (a) TRMC signals versus time recorded for CB-Cu<sub>2</sub>O and RD-Cu<sub>2</sub>O at a photo flux of  $8.0 \times 10^{12}$  photon pulse<sup>-1</sup> cm<sup>-2</sup> with zoom in conductance plot of CB-Cu<sub>2</sub>O (inset) and (b) maximum photoconductance plot versus pulse intensity using 532 nm laser pulse.

### Dark-microwave conductivity measurement procedure

A similar system as the TRMC was retained for this measurement apart from the laser pulse irradiation. In this instance, no laser pulse was directed to the cavity holding the samples, and the samples were therefore not excited. By assuming that the small perturbation condition is maintained, the change in the conductance of Cu<sub>2</sub>O can be calculated according to Equation S1.

$$\frac{\Delta P_{Cu_2O/quartz} - \Delta P_{quartz}}{P}(t) = \frac{\Delta P}{P} = -K\Delta G(t) \quad (S1)$$

where  $\Delta P/P$  is the change in normalized reflected dark microwave power of the quartz to the Cu<sub>2</sub>O sample deposited on quartz in the cavity and K is the sensitivity factor.

By measuring the  $\Delta P/P$ , the conductivity ( $\sigma$ ) and carrier concentration ( $N_a$ ) can be calculated according to Equation S2 and S3.

$$\Delta G = \Delta\sigma\beta d \quad (S2)$$

$$\Delta\sigma = eN_a\mu_e \quad (S3)$$

where  $\beta$  is the ratio between the inner broad and narrow dimensions of the waveguide, e is the elementary charge, d is the thickness of the film and  $\mu$  is the effective carrier mobility (obtained from the TRMC measurements with laser pulse illumination).

**Table S2** illustrated the calculated carrier concentrations of CB-Cu<sub>2</sub>O and RD-Cu<sub>2</sub>O based on three repeated dark microwave conductivity measurements of three different thin films. These results consistently demonstrated that RD-Cu<sub>2</sub>O has lower conductivity and lower carrier concentration when compared to CB-Cu<sub>2</sub>O.

**Table S3:** Parameters involved in dark microwave conductivity measurement.

Samples	$\Delta P/P_0$	K	$\Delta G$ (S)	$\Delta\sigma$ (S/cm)	$\mu$ ( $\text{cm}^2\text{V}^{-1}\text{s}^{-1}$ )	$N_a$ ( $\text{cm}^{-3}$ )
CB-Cu <sub>2</sub> O	-0.2139	8881	0.00002	1.07	0.006	$1.20 \times 10^{21}$
	-0.2550	8973	0.00003	1.26	0.008	$9.96 \times 10^{20}$
	-0.2860	8957	0.00003	1.41	0.006	$1.49 \times 10^{21}$
RD-Cu <sub>2</sub> O	-0.0648	7788	0.00001	0.37	0.193	$1.19 \times 10^{19}$
	-0.0974	8251	0.00001	0.52	0.206	$1.59 \times 10^{19}$
	-0.1003	8765	0.00001	0.51	0.210	$1.51 \times 10^{19}$

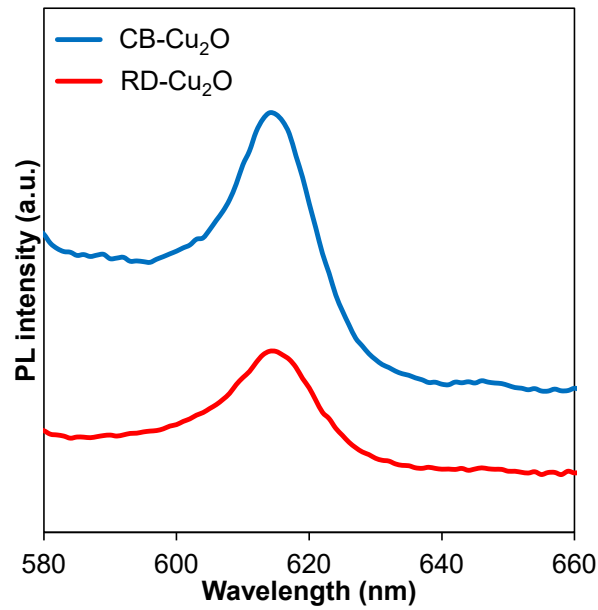


**Figure S5:** Steady-state photoluminescence spectra of CB-Cu<sub>2</sub>O and RD-Cu<sub>2</sub>O.

## Surface photovoltage spectroscopy (SPV) measurement

**Figure S6a** shows modulated SPV spectra of in-phase and phase-shifted by  $90^\circ$  signals of CB-Cu<sub>2</sub>O measured at 5, 15 and 80 Hz. The SPV signals set on strongly at about 2 eV (the band gap of Cu<sub>2</sub>O), but already starting to appear at lower photon energies (defect range). The SPV signals reached a first maximum at about 2.2 eV, a local minimum at about 2.5 eV and a second maximum at about 2.75 eV and decrease at higher photon energies due to decreasing light intensity. The appearance of minima and maxima in the range of fundamental absorption points to a strong influence of the penetration depth of light on the mechanism(s) of charge separation and relaxation. With increasing frequency, the in-phase signals decreased whereas the shapes of the modulated SPV spectra of CB-Cu<sub>2</sub>O did not change qualitatively. However, the in-phase signals in the maximum at 2.2 eV decreased stronger with increasing frequency than the signals in the maximum at 2.75 eV.

Similarly, **Figure S6b** signifies the modulated SPV spectra of in-phase and phase-shifted by  $90^\circ$  signals of RD-Cu<sub>2</sub>O measured at 5, 15 and 80 Hz. Surprisingly, the SPV signals of RD-Cu<sub>2</sub>O were much lower than the SPV signals of CB-Cu<sub>2</sub>O by up to two orders of magnitude. The in-phase signals of RD-Cu<sub>2</sub>O were negative for measurements at 5 Hz. At higher frequencies, the spectra of the in-phase signals changed qualitatively. For in-phase signals at higher frequencies, a strong decrease with negative sign set on at 2.15 eV, continued to an increase of signals with positive sign with a positive maximum at 2.6 eV and decreased towards negative signals at higher photon energies. The very low modulated SPV signals and the change of the sign gave evidence for competing processes of charge separation in RD-Cu<sub>2</sub>O, whereas both processes were rather similar in their efficiency according to modulated charge separation.

The frequency dependencies of the SPV amplitudes of CB-Cu<sub>2</sub>O (**Figure 7a**) could be well fitted with a sum of two exponentials (Equation S4).

$$R(f_{mod}) = A_1 \cdot \exp\left(-\frac{f_{mod}}{f_{mod,1}}\right) + A_2 \cdot \exp\left(-\frac{f_{mod}}{f_{mod,2}}\right) \quad (S4)$$

All dependencies were fitted with the same values of  $f_{mod,1}$  (300 Hz) and  $f_{mod,2}$  (20 Hz) corresponding to time constants  $\tau_1$  and  $\tau_2$  of 3.3 and 50 ms, respectively. The amplitude of the “slow” process ( $A_1$ ) saturated at higher photon energies. In contrast, the amplitude of the “fast” ( $A_2$ ) process increased permanently with increasing photon energy.

In contrast to CB-Cu<sub>2</sub>O, the frequency dependencies of the SPV amplitudes of RD-Cu<sub>2</sub>O could not be well fitted with a sum of two exponentials but with a sum of one exponential and a second exponential multiplied with a logistic growth function (Equation S5).

$$R(f_{mod}) = A_1 \cdot \exp\left(-\frac{f_{mod}}{f_{mod,1}}\right) \cdot \frac{1}{1 + \exp\left(-\frac{f_{mod} - f_{mod,on}}{f_{mod,g}}\right)} + A_2 \cdot \exp\left(-\frac{f_{mod}}{f_{mod,2}}\right) \quad (S5)$$

In difference to CB-Cu<sub>2</sub>O, the frequency dependencies of RD-Cu<sub>2</sub>O could not be fitted with constant values of  $f_{mod,1}$  and  $f_{mod,2}$ . In addition, also the onset frequency ( $f_{mod,on}$ ) and the frequency characterizing the exponential growth ( $f_{mod,g}$ ) could not be kept constant during the fitting. The values for fitting the frequency dependencies at 1.8, 2.0, 2.5 and 2.7 eV were about 45, 84, 124, 160 Hz ( $f_{mod,1}$ ), 10, 8, 8, 5 Hz ( $f_{mod,2}$ ), 50, 44, 41, 50 Hz ( $f_{mod,on}$ ) and 10, 43, 43, 70 Hz ( $f_{mod,g}$ ), respectively. This means that all time constants corresponding to the “fast” process, i.e.  $f_{mod,1}$  and  $f_{mod,g}$ , decreased with increasing photon energy. One has to keep in mind that the time constant of the “slow” process can be considered as practically constant due to the relatively large experimental error for the measurement at the lowest frequency.

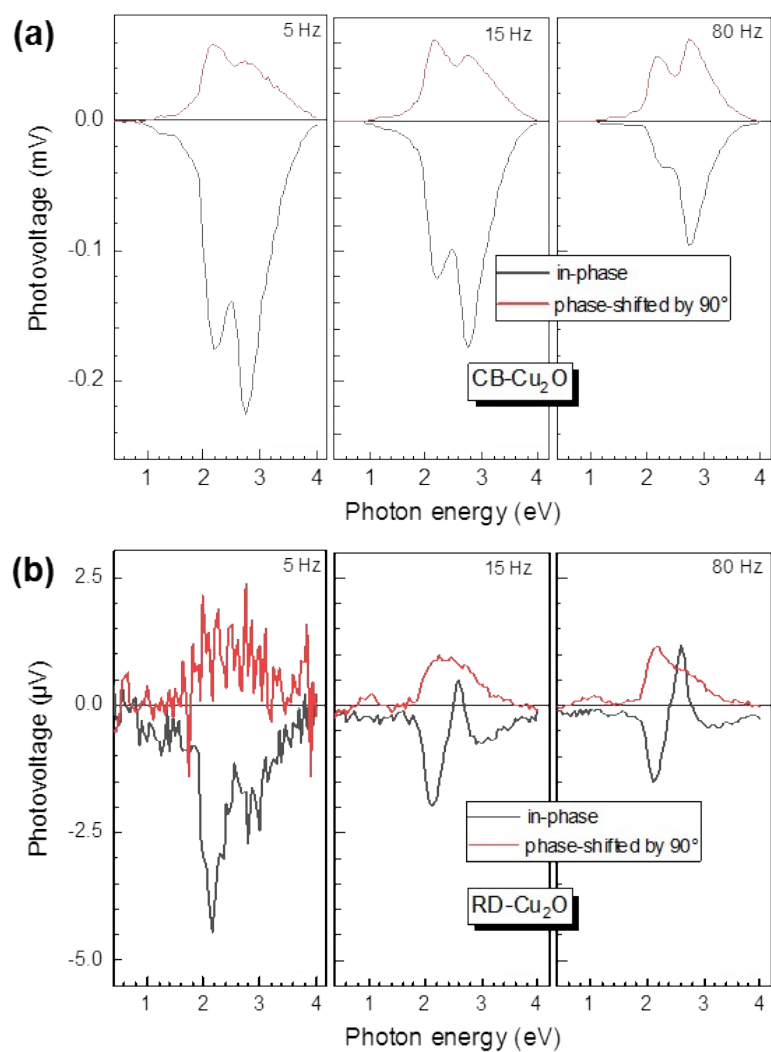


**Figure S6:** Modulated SPV spectra of in-phase (dark grey) and phase-shifted by 90° (red) signals measured at modulation frequencies of 5, 15 and 80 Hz for (a) CB-Cu<sub>2</sub>O and (b) RD-Cu<sub>2</sub>O.

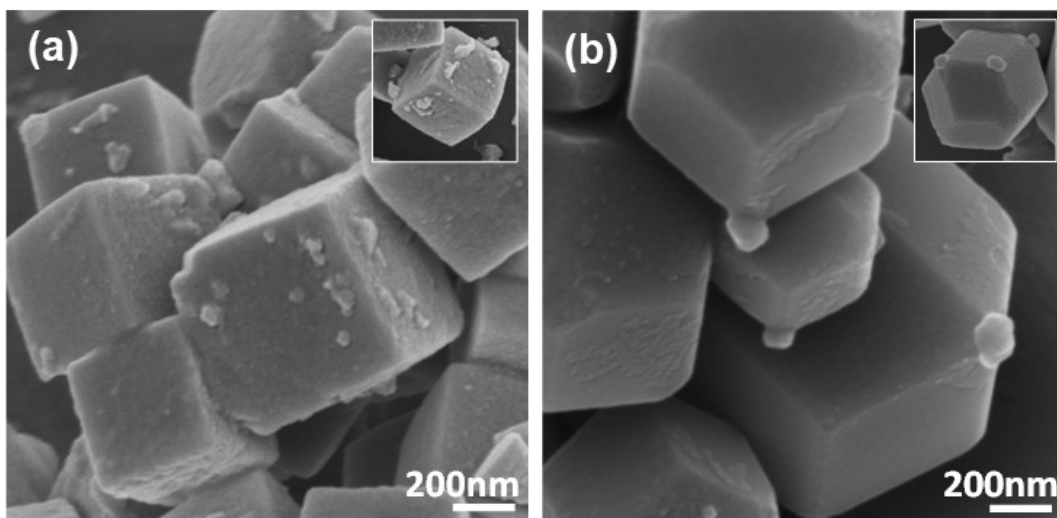


**Figure S7:** SEM images of (a) CB-Cu<sub>2</sub>O and (b) RD-Cu<sub>2</sub>O after photodeposition of Ag nanoparticles with insets, the corresponding views on a single particle.

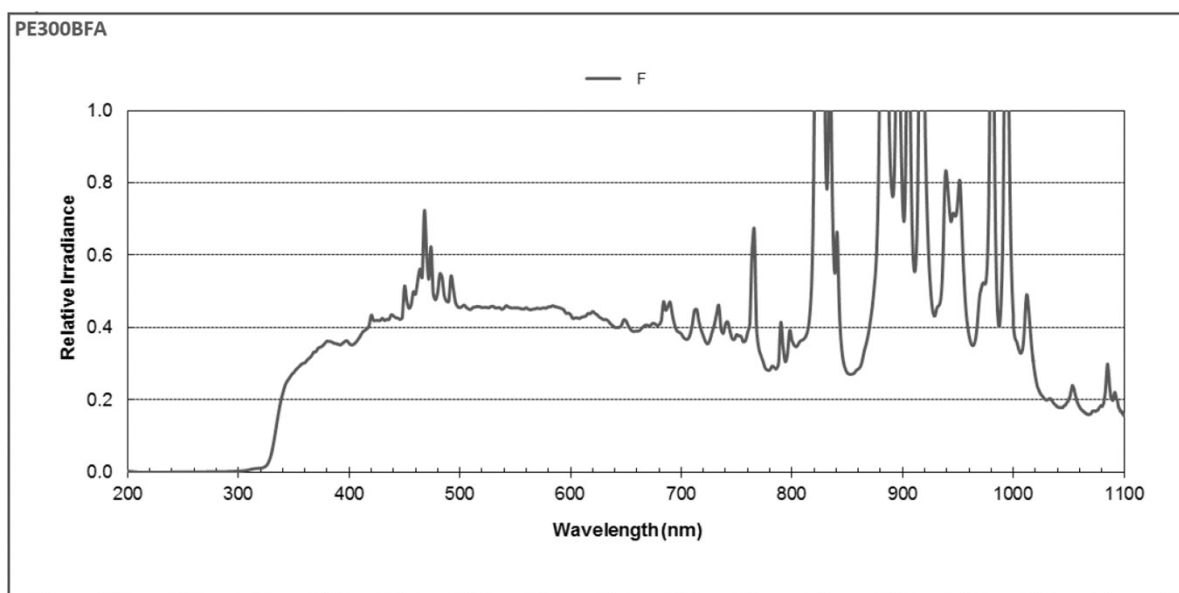


**Figure S8:** Light spectral output of CERMAX<sup>®</sup> xenon arc lamp (PE300BFA) used in this study. Spectral output is obtained from Excelitas Technologies's Data Sheet Lighting Solutions for CERMAX<sup>®</sup> Xenon Arc Lamp (PE300BFA). © 2012 Excelitas Technologies Corp. (<https://www.excelitas.com/>)

## Reference:

- S1. L. Zhang, J. Shi, M. Liu, D. Jing and L. Guo, *Chem. Commun.*, 2014, **50**, 192-194.
- S2. Y.-H. Zhang, Y.-L. Li, B.-B. Jiu, F.-L. Gong, J.-L. Chen, S.-M. Fang and H.-L. Zhang, *Nanotechnology*, 2019, **30**, 145401.
- S3. B. Zhuang, L. Xiangqing, R. Ge, S. Kang, L. Qin and G. Li, *Appl. Catal., A*, 2017, **533**, 81-89.
- S4. S. Bai, J. Ge, L. Wang, M. Gong, M. Deng, Q. Kong, L. Song, J. Jiang, Q. Zhang and Y. Luo, *Adv. Mater.*, 2014, **26**, 5689-5695.
- S5. Y. Kwon, A. Soon, H. Han and H. Lee, *J. Mater. Chem. A*, 2015, **3**, 156-162.
- S6. S. McWilliams, C. D. Flynn, J. McWilliams, D. C. Arnold, R. A. Wahyuono, A. Undisz, M. Rettenmayr, A. Ignaszak, *Nanomaterials*, 2019, **9**, 1781.
- S7. C. Y. Toe, Z. Zheng, H. Wu, J. Scott, R. Amal and Y. H. Ng, *Angew. Chem., Int. Ed.*, 2018, **57**, 13613-13617.